Electrical Power and Energy Systems 153 (2023) 109394

Contents lists available at ScienceDirect

International Journal of Electrical Power and Energy Systems

journal homepage: www.elsevier.com/locate/ijepes

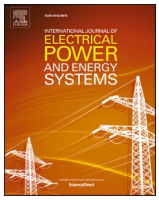

Low voltage ride-through augmentation of DFIG wind turbines by simultaneous control of back-to-back converter using partial feedback linearization technique

M.A. Chowdhury [a], G.M. Shafiullah [b,*], S.M. Ferdous [b]

[a] FIMER Australia, VIC 3072, Australia
[b] School of Engineering and Energy, Murdoch University, WA 6150, Australia

ARTICLE INFO

Keywords:
Doubly fed induction generators
Partial feedback linearization
Nonlinear control
Low voltage ride-through capability

ABSTRACT

This paper proposes a nonlinear controller for doubly fed induction generator (DFIG) wind turbines using partial feedback linearization (PFL) technique. The controller generates switching signals for driving both the rotor side converter and grid side converter simultaneously enhancing the low voltage ride through (LVRT) capability over a wide range of operating conditions. The proposed PFL method has been implemented into a partially linearized form of a nonlinear system, where the transformed system has been made autonomous and reduced in order. All calculations in the proposed method except for the control laws have been carried out offline resulting in reduced design and implementation complexity, small computational burden, and offline control tuning with fast tracking performances. The step-by-step approach of control design and implementation includes system modeling and partial linearization, control law derivation, software implementation, and controller tuning. The effectiveness of the proposed controller has been evaluated through electromagnetic transient simulations. The simulations have demonstrated that the controller has successfully augmented the LVRT capability of DFIG wind turbines and has remained robust against diverse wind conditions and voltage sags.

1. Introduction

Wind energy is experiencing the highest penetration among renewable energy sources in recent years [1]. Owing to the lower cost of power converters, DFIG has become an extensively popular option for wind power generation. Thus, DFIG wind turbines have captured a significant market share among all other technologies [2]. However, the gearbox that couples the DFIG and the wind turbine experience longer downtime when it is damaged. Overhauling the coupling system is also complicated [3]. Furthermore, the stator of the DFIG being directly connected to the grid is highly sensitive to low voltage conditions [4]. This introduces a DC component of natural flux in the stator windings, which rotates with the rotor windings synchronously at rotor speed. It consequently results in an electromotive force in the rotor that may be large enough to cause saturation to the rotor side converter (RSC) and make LVRT challenging for DFIG wind turbines [5]. Furthermore, a large transient rotor current may be induced, which may cause the DC-link voltage to increase to a level that may exceed the safety limits of the semiconductor switches. This poses potential risk of damaging the converters. A negative sequence stator flux may be produced along with natural stator flux during asymmetrical faults, making the scenario even worse [6]. The electromagnetic torque in the rotor may encounter oscillations causing mechanical stress on the turbine blades and shafts. This may eventually reduce the gearbox's lifespan and reliability [7]. Moreover, the wind turbine may experience overspeed conditions, which may pose risks to the turbine's mechanical components and overall system integrity. Thus, with an increasing share of wind energy, low voltage ride-through (LVRT) capability of DFIG wind turbines has become one of the most import requirements in the grid code [8]. This requirement enforces the DFIG wind turbines to remain connected to the grid during low voltage conditions for a certain period to support the grid. This introduces new challenges for manufacturers, proponents, and grid operators as they strive to meet the updated LVRT requirements [6]. As a result, LVRT augmentation strategy has grasped a core research focus in academia and industries [9].

Over the years of research, researchers have come up with several modern control strategies that can be categorized as hardware (external

* Corresponding author.
E-mail addresses: ayaz.chowdhury@fimer.com (M.A. Chowdhury), GM.Shafiullah@murdoch.edu.au (G.M. Shafiullah), SM.Ferdous@murdoch.edu.au (S.M. Ferdous).

https://doi.org/10.1016/j.ijepes.2023.109394
Received 9 November 2022; Received in revised form 18 May 2023; Accepted 22 July 2023
Available online 28 July 2023

Nomenclature

T_{ae}	Aerodynamic torque
T_m	Mechanical torque
T_e	Electromagnetic torque
ω_m	Rotor shaft angular speed
ω_r	Generator rotor angular speed
H	Inertia constant
K_s	Torsion stiffness
γ	Torsion angle
D	Torsion damping coefficient
f	Grid frequency
ω_o	Natural angular speed
N_g	Gear ratio
I_r, V_r	Current and voltage in the RSC loop
R_{rf}, L_{rf}	Resistance and inductance of the RSC filter
I_g, V_g	Current and voltage in the GSC loop
R_{gf}, L_{gf}	Resistance and inductance of the GSC filter
I_s, V_s, R_s, L_s	Current, voltage, resistance and inductance in the stator circuit
i_{dc}, v_{dc}, C	Current and voltage and capacitance in the DC-link circuit
I, V, R, L	Current, voltage (at Point of Common Coupling, i.e. PCC), resistance and inductance of the transmission line
L_{tr}	Inductance of the transformer
V_{TH_LVRT}	Voltage threshold for LVRT
K_{RSC_LVRT}	RSC gain constant for LVRT
K_{GSC_LVRT}	GSC gain constant for LVRT
E	Grid voltage
S	Input switching signals for the DFIG converters
P	Active power exchange between the DFIGs and the grid
Q	Reactive power exchange between the DFIGs and the grid
r	Relative degree with respect to control outputs
n	System order
A	System matrix of the linearized system
B	Input matrix of the linearized system
v	Linear control input of the linearized system
$\widetilde{A}$	System matrix of the partially linearized system
$\widetilde{B}$	Input matrix of the partially linearized system
$\widetilde{v}$	Linear control input of the partially linearized system
V_W	Wind speed

circuits, components, or/and converters), software, or a combination of both strategies. The combination of hardware and software is commonly referred to as an improved control strategy incorporating one or more Energy Storage Systems (ESS) [6]. A modified linear quadratic output-feedback decentralized controller has been used in [10], where the robustness has been assessed utilizing the higher-order terms in Taylor's series as uncertainty. In [11], an advanced control method for the grid side converter (GSC) has been applied that may efficiently absorb postfault kinetic energy to damp system oscillations. The overcurrent during low voltage conditions is effectively damped by limiting the overshoot of rotor current by using feedforward and stator current control [12]. Nevertheless, overvoltage may still be present on the RSC circuit during voltage dip even with the application of advanced control strategies. This happens due to constraints on RSC's voltage capacity imposed by the DC-link voltage [13]. In order to address such problems, researchers have started utilizing the technology of power electronic devices. For example, a DC chopper has been used to limit the DC-link voltage [14]. Superior performance has been achieved through hardware modifications in [15]. The modification includes the insertion of a resistance to limit the rotor transient overcurrent during low voltage conditions. The dynamic voltage restorer (DVR) has also been used to restore the terminal voltage [16]. A real-time static synchronous compensator (STATCOM) has been designed and coordinated with DFIG converters in [17] to assist with uninterrupted DFIG operation. However, this solution has come with a substantial cost.

As a more cost-effective alternative, the rotor side crowbar has been widely adopted for enhancing the LVRT capability of DFIG wind turbines [18]. A coordinated control approach has been employed for the crowbar connected to the rotor side of the DFIG to bypass the RSC from overshooting of rotor current and consequently dampen the stator natural flux [19]. The grid compliance codes, however, enforce that the crowbar must be turned OFF within 100 ms of the fault occurrence and the RSC provides necessary reactive power support to the grid [20]. The role of the crowbar has become insignificant (i.e., no further triggering of the crowbar) when the post-fault stator natural flux has become trivial [21]. The DFIG may still fail to perform LVRT even with the crowbar installed if the overshoot in the rotor current cannot be properly minimized. This would result in fluctuating stator natural flux and thus electromagnetic torque consequently. This would highly influence the reliability of the mechanical system [22]. An efficient RSC control approach has been instrumental in reducing both positive- and negative-sequence components of the rotor current [23].

Nonlinear Controllers are inherently robust offering an effective solution to the LVRT problems. Such controllers are effectively implementable in any existing wind turbine as they do not require any additional hardware. However, a superior performance may still be attained with a nonlinear controller integrated with an additional hardware based LVRT strategy [24]. One of the key advantages of using a nonlinear controller is that a nonlinear model of the system is considered. Hence, the designed controllers are independent of operating conditions making them robust to parameter variations, model uncertainties and disturbances. A direct model reference adaptive internal model controller based LVRT technique has been proposed in [25], where the rotor current has been controlled by variable gain adjustments using fuzzy sets. Using the rotor inertia to store the surplus energy during low voltage conditions, a model predictive control mechanism has been discussed in [26]. A model predictive controller based on two stage coordinated DC link voltage control with supercapacitor storage has been proposed for fast reactive power support during grid voltage swell without a DC chopper [27]. The concept of model predictive control has been modified by incorporating a fuzzy control in [28], which has offered better performance of the DFIGs during LVRT. A state estimation technique has been implemented in [29] to enhance the LVRT capability, which has minimized the effect of noise in parameter measurements. To provide robustness in parametric uncertainties, nonlinear adaptive backstepping controllers for DFIG have been proposed that may provide good reactive power support to the grid during low voltage conditions [30]. This type of controller has the capability to mitigate oscillations in active and reactive powers, as well as stabilize DC link voltage. The sliding mode control (SMC) technique has been used for LVRT in [31], which has outperformed the conventional PI controller in terms of reducing overshoot, transient time, and dynamic response [32]. Incorporating additional hardware along with SMC has further enhanced the LVRT capability [33]. A fuzzy second order SMC for RSC and GSC along with an additional series GSC has been used for LVRT in [34]. Such an additional GSC helps limit the stator and rotor current within a limit of 10 % and DC link voltage within 2 % of the peak value. A fuzzy PI-based approach has been proposed in a hybrid system in [35], where the DC link of the RSC and GSC have been connected to the system via a DC-DC converter. During low voltage conditions, the GSC operates as STATCOM to provide reactive power support to the grid while the DC-DC converter regulates the DC-link

voltage. A cascaded converter has been incorporated to augment the LVRT capability as well as improve overall stability of the DFIG system [36].

Several pure control solutions for the LVRT technique without any auxiliary hardware have also been proposed in the literature. A nonlinear controller using both feedforward and feedback terms has been employed for enhancing asymmetric LVRT capability without any auxiliary protection hardware [37]. An LVRT strategy based on flux linkage tracking has been proposed to suppress the short-circuit rotor current, which has been achieved with no additional hardware device [38].

Partial Feedback linearization (PFL) is a straightforward method to design nonlinear controllers [39]. Compared to other nonlinear control methods in the literature, the proposed approach offers a simplified design and implementation method as it does not require complete knowledge of the system dynamics. Instead, it performs a partial linearization of the non-linear system. Moreover, all calculations except for the control laws comprising four nonlinear equations are carried out offline resulting in reduced control design complexity. This control method utilizes a reduced-order model of the wind turbine system enabling the controller to focus only on the most significant system states and inputs. This method does not necessitate complex inverse functions or matrices computation. A few nonlinear equations require a real-time solution allowing a small computational burden and offline controller tuning with fast tracking performance. A PFL controller has been proposed by the authors in [40] generating signals to drive the RSC alone to mitigate subsynchronous resonance (SSR) in series-compensated DFIG wind turbines. Meanwhile, a nonlinear control concept using PFL technique has been proposed in this paper with the following state-of-the-art features:

(i) the controller generates switching signals for driving both the RSC and the GSC simultaneously.
(ii) the controller utilizes the PFL technique in augmenting the symmetric and asymmetric LVRT capabilities for DFIG wind turbines.
(iii) the controller is robust, independent of the operating point, and capable of functioning under parametric variations and disturbances.
(iv) the controller adapts itself to any existing wind farm as it does not require additional hardware/components/converters or ESS; only software change will be adequate to implement the controller at no further cost, making it an economically viable solution.

Electromagnetic transient simulations have been performed to show that the controller has successfully augmented the LVRT capability of DFIG wind turbines and has remained robust against diverse wind conditions and voltage sags. A comparative analysis of different LVRT techniques and their key features with the proposed research has been illustrated in Table 1.

The rest of the paper has been structured as follows: Dynamic model of a test system integrated with DFIG wind turbines has been presented in Section 2. A systematic design approach of the proposed controller has been explained in Section 3. The software implementation of the proposed control scheme has been discussed in Section 4. The performance of the proposed controller has been demonstrated in Section 5. The conclusions have finally been drawn in Section 6.

2. Power system dynamic model

This section presents a dynamic model of a test system integrated with DFIG wind turbines. A simplified Nordic power grid has been adopted from Ref. [41] with penetration of 148 MW of active power at the point of common coupling (PCC) generated from 74 DFIG units (each with a power rating of 2 MW). An aggregated model has been used to represent DFIG wind turbines supplying to the grid. The aggregation technique in this paper has been adopted from Ref. [42]. Fig. 1 shows a diagram of a simplified Nordic grid integrated with aggregated DFIG wind turbines.

The wind turbine generates aerodynamic torque from the incoming wind speed. A two-stage torque conversion takes place in the gearbox, which can suitably be demonstrated through the following first-order derivative equations (known as two-mass shaft dynamics):

$$\dot{\omega}_m = \frac{1}{2H_t}(T_{ae} - K_s\gamma - D_t\omega_m)$$

$$\dot{\omega}_r = \frac{1}{2H_g}\left(K_s\gamma - T_{ae} - D_g\omega_r\right)$$

$$\dot{\gamma} = 2\pi f\left(\omega_m - \frac{1}{N_g}\omega_r\right) \quad (1)$$

where subscript 't' and 'g' denote turbine and generator, respectively.

On the other hand, the electrical dynamics in the loop of power electronic converters are mathematically expressed as [43]:

$$\dot{I}_{rq} = \omega_o I_{rd} + \frac{R_{rf}}{L_{rf}}I_{rq} + \frac{V_{rq}}{L_{rf}} - \frac{v_{dc}}{L_{rf}}S_{rq}$$

$$\dot{I}_{rd} = \frac{R_{rf}}{L_{rf}}I_{rd} - \omega_o I_{rq} + \frac{V_{rd}}{L_{rf}} - \frac{v_{dc}}{L_{rf}}S_{rd}$$

Table 1
Comparison of different LVRT techniques.

LVRT Features	LVRT Techniques												
	Hardware-based					Software based				Combination			Proposed
	[2]	[4]	[15]	[16]	[20]	[25]	[26]	[31]	[38]	[6]	[32]	[34]	
External Hardware	Y	Y	Y	Y	Y	N	N	N	N	Y	Y	Y	**N**
Adaptability in an existing system	N	N	N	N	N	Y	Y	Y	Y	N	N	N	**Y**
Cost Economic	N	N	N	N	N	Y	Y	Y	Y	N	N	N	**Y**
High Computational Complexity	N	N	N	Y	N	Y	Y	Y	Y	Y	Y	Y	**N**
Robustness	N	N	Y	Y	N	N	Y	N	N	Y	N	Y	**Y**
Parameter Variation	N	N	Y	Y	N	N	N	Y	Y	Y	N	Y	**Y**
Model Uncertainties	N	N	N	N	N	N	N	Y	Y	Y	N	Y	**Y**
ESS	N	Y	Y	Y	N	N	N	N	N	N	N	N	**N**
Mechanical Stress	Y	N	Y	N	Y	Y	Y	Y	Y	Y	Y	N	**N**
Active Power Support	N	Y	Y	Y	N	N	N	N	N	N	N	N	**N**
Reactive Power Support	N	Y	N	Y	N	N	N	N	N	N	N	N	**Y**

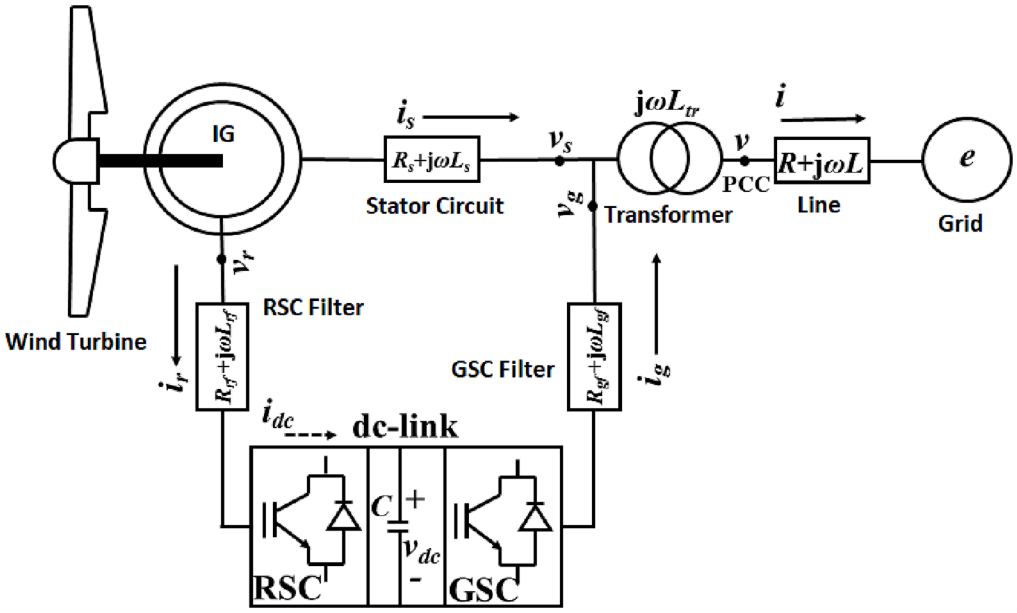

Fig. 1. Simplified Nordic grid integrated with aggregated DFIG wind turbines.

$$\dot{I}_{gq} = -\omega_o I_{gd} - \frac{R_{gf}}{L_{gf}} I_{gq} - \frac{V_{gq}}{L_{gf}} + \frac{v_{dc}}{L_{gf}} S_{gq}$$

$$\dot{I}_{gd} = -\frac{R_{gf}}{L_{gf}} I_{gd} + \omega_o I_{gq} - \frac{V_{gd}}{L_{gf}} + \frac{v_{dc}}{L_{gf}} S_{gd}$$

$$\dot{v}_{dc} = \frac{1}{C} i_{dc} - \frac{1}{C} I_{gq} S_{gq} - \frac{1}{C} I_{gd} S_{gd} \tag{2}$$

A simplification in the rotor current is made neglecting the machine's electromagnetic dynamics. This is done to facilitate the control design based on the partially linearized form of the system that decouples the electromagnetic dynamics from the control design.

Similarly, electrical dynamic equations on the stator side can be written as:

$$\dot{I}_{sq} = -\omega_o I_{sd} + \frac{R_s}{L_s} I_{sq} + \frac{V_{sq}}{L_s}$$

$$\dot{I}_{sd} = \frac{R_s}{L_s} I_{sd} + \omega_o I_{sq} + \frac{V_{sd}}{L_s} \tag{3}$$

and in the transmission line side as:

$$\dot{I}_q = -\omega_o I_d + \frac{R}{L + L_{tr}} I_q + \frac{1}{L + L_{tr}} (V_q - E_q)$$

$$\dot{I}_d = \frac{R}{L + L_{tr}} I_d + \omega_o I_q + \frac{1}{L + L_{tr}} (V_d - E_d) \tag{4}$$

The power exchange between the DFIGs and the grid can be represented as follows:

$$P = \frac{3}{2} \left(V_{sq} I_{sq} + V_{sd} I_{sd} + V_{gq} I_{gq} + V_{gd} I_{gd} \right)$$

$$Q = \frac{3}{2} \left(V_{sq} I_{sd} + V_{sd} I_{sq} + V_{gq} I_{gd} + V_{gd} I_{gq} \right) \tag{5}$$

This paper mainly aims at designing a nonlinear current controller for the DFIG converters using the PFL technique to augment the LVRT capability of DFIG wind turbines. The controller will simultaneously generate control input signals, S_{rq} and S_{rd} for switching RSC, and S_{gq} and S_{gd} for GSC.

3. Controller design

A systematic design approach of the proposed controller has been explained in this section. Power electronic converters in DFIGs may encounter potential damage due to grid faults. Hence, the proposed controller must be capable of minimizing overshoot in rotor current as well as maintaining DC-link voltage, v_{dc} to the nominal value. Thus, I_{rq}, and I_{rd} are chosen as control objectives for driving RSC switches while I_{gq}, and v_{dc} are chosen for driving GSC switches.

To facilitate controller design and implementation to a partially linearized system, the power system equations (1)-(4) mentioned in Section 2 are represented in the following MIMO form:

$$\dot{x} = f(x) + \sum_{i=1}^{4} g_i(x) u_i$$

$$y_1 = h_1(x)$$

$$y_2 = h_2(x)$$

$$y_3 = h_3(x)$$

$$y_4 = h_4(x) \tag{6}$$

where

$$x = [\omega_m \quad \omega_r \quad \gamma \quad I_{rq} \quad I_{rd} \quad I_{gq} \quad I_{gd} \quad v_{dc} \quad I_{sq} \quad I_{sd} \quad I_q \quad I_d]^T$$

$$u = [S_{rq} \quad S_{rd} \quad S_{gq} \quad S_{gd}]^T$$

$$y = [I_{rq} \quad I_{rd} \quad I_{gq} \quad v_{dc}]^T$$

$$f(x)=\begin{bmatrix}\frac{1}{2H_t}(T_{ae}-K_s\gamma-D_t\omega_m)\\ \frac{1}{2H_g}(K_s\gamma-T_{ae}-D_g\omega_r)\\ \dot{\gamma}=2\pi f\left(\omega_m-\frac{1}{N_g}\omega_r\right)\\ \omega_o I_{rd}+\frac{R_{rf}}{L_{rf}}I_{rq}+\frac{V_{rq}}{L_{rf}}\\ \frac{R_{rf}}{L_{rf}}I_{rd}-\omega_o I_{rq}+\frac{V_{rd}}{L_{rf}}\\ -\omega_o I_{gd}-\frac{R_{gf}}{L_{gf}}I_{gq}-\frac{V_{gq}}{L_{gf}}\\ -\frac{R_{gf}}{L_{gf}}I_{gd}+\omega_o I_{gq}-\frac{V_{gd}}{L_{gf}}\\ \frac{i_{dc}}{C}\\ -\omega_o I_{sd}+\frac{R_s}{L_s}I_{sq}+\frac{V_{sq}}{L_s}\\ \frac{R_s}{L_s}I_{sd}+\omega_o I_{sq}+\frac{V_{sd}}{L_s}\\ -\omega_o I_d+\frac{R}{L+L_{tr}}I_q+\frac{1}{L+L_{tr}}(V_q-E_q)\\ \frac{R}{L+L_{tr}}I_d+\omega_o I_q+\frac{1}{L+L_{tr}}(V_d-E_d)\end{bmatrix}$$

and

$$g(x)=\begin{bmatrix}0&0&0&0\\0&0&0&0\\0&0&0&0\\-\frac{v_{dc}}{L_{rf}}&0&0&0\\0&-\frac{v_{dc}}{L_{rf}}&0&0\\0&0&\frac{v_{dc}}{L_{gf}}&0\\0&0&0&0\\0&0&-\frac{I_{gq}}{C}&-\frac{I_{gd}}{C}\\0&0&0&0\\0&0&0&0\\0&0&0&0\\0&0&0&0\end{bmatrix}$$

Let us consider that the system (6) has state z, which can be expressed in its corresponding nonlinear coordinate transformed form as follows:

$$z=\left[h_i \quad L_f h_i \quad \ldots \quad L_f^{r_i-1}h_i\right]^T; i=1,\,2,\,3,\,4$$

where $L_f\, h_i(x)$ is the Lie derivative of $h_i(x)$ along $f(x)$.

Lie derivative transforms the nonlinear system (6) with the state vector x into a linear dynamic system with the state vector z provided that the following conditions are satisfied for $n=(r_1+r_2+r_3+r_4)$ [41]:

$$L_g L_f^{r_i-1}h_i(x)\neq 0; i=1,\,2,\,3,\,4$$

where $L_{gi}\, L_f\, h_i(x)$ is the Lie derivative of $L_f\, h_i(x)$ along $g(x)$.

Upon meeting the conditions, a linear controller can be implemented in the following linearized system, whose dynamics can be modeled by a set of linear differential equations:

$$\dot{z}=Az+Bv \tag{9}$$

where the input v is applied linearly to the system through the input matrix B. The state variables z describes the current state of the system, and their evolution is governed by the state matrix A. Thus, a linear controller can be designed to operate on the state variables z and produce the input v to achieve the desired system behavior.

We can do partial linearization only if $(r_1+r_2+r_3+r_4)<n$ and in this case, the transformed states z can be expressed as a function of the state variables x as follows:

$$z=\varphi(x)=[\tilde{z}\quad \hat{z}]^T \tag{10}$$

where $\tilde{z}$ is the transformed state (through nonlinear coordination) of the order of $(r_1+r_2+r_3+r_4)$, and $\hat{z}$ is the transformed state related to the remaining n-$(r_1+r_2+r_3+r_4)$-th order.

We can now represent the partially linearized system as follows:

$$\dot{\tilde{z}}=\tilde{A}\tilde{z}+\tilde{B}\tilde{v} \tag{11}$$

We can implement the linear controller to the partially linearized system only if the stability of internal dynamics of the system is proven to be stable. Examination in Ref. [39] assures the stability of the internal dynamics of our studied system, which can be represented as:

$$\dot{\hat{z}}=\hat{A}\hat{z}+\hat{B}\hat{v} \tag{12}$$

Partial linearizability of the power system (1)-(4) can be attained by computing relative degrees with respect to the output functions. The relative degrees with respect to $h_1(x)=I_{rq}$, $h_2(x)=I_{rd}$, $h_3(x)=I_{gq}$, and $h_4(x)=v_{dc}$, can be computed by performing following operations.

$$L_g L_f^{1-1}h_1(x)=L_g h_1(x)=-\frac{v_{dc}}{L_{rf}}S_{rq}\neq 0$$

$$L_g L_f^{1-1}h_2(x)=L_g h_2(x)=-\frac{v_{dc}}{L_{rf}}S_{rd}\neq 0$$

$$L_g L_f^{1-1}h_3(x)=L_g h_3(x)=\frac{v_{dc}}{L_{gf}}S_{gd}\neq 0$$

$$L_g L_f^{1-1}h_4(x)=L_g h_4(x)=-\frac{1}{C}\left(I_{gq}S_q+I_{gd}S_d\right)\neq 0 \tag{13}$$

It indicates that the relative degree for each of the outputs is 1, which makes $(r_1+r_2+r_3+r_4)=4$, which is less than the system order n (where $n=12$).

Thus, the studied power system is partially linearizable with respect to the output functions. To do partial linearization to the system, a nonlinear coordinate transformation can be done as follows:

$$\tilde{z}=\tilde{\varphi}(x) \tag{14}$$

For the studied power system, we choose.

$$\tilde{z}_1=\tilde{\varphi}_1(x)=h_1(x)=I_{rq} \tag{15}$$

Similarly, we have

$$\tilde{z}_2=I_{rd}$$

$$\tilde{z}_3=I_{gq}$$

$$\tilde{z}_4=v_{dc} \tag{16}$$

Now, the partial feedback linearized system can be written as [39].

$$\dot{\tilde{z}}_1=\frac{\partial h_1(x)}{\partial x}\dot{x}=\omega_o I_{rd}+\frac{R_{rf}}{L_{rf}}I_{rq}+\frac{V_{rq}}{L_{rf}}-\frac{v_{dc}}{L_{rf}}S_{rq}$$

$$\dot{\tilde{z}}_2=\frac{\partial h_2(x)}{\partial x}\dot{x}=\frac{R_{rf}}{L_{rf}}I_{rd}-\omega_o I_{rq}+\frac{V_{rd}}{L_{rf}}-\frac{v_{dc}}{L_{rf}}S_{rd}$$

$$\dot{\tilde{z}}_3=\frac{\partial h_3(x)}{\partial x}\dot{x}=-\omega_o I_{gd}-\frac{R_{gf}}{L_{gf}}I_{gq}-\frac{V_{gq}}{L_{gf}}+\frac{v_{dc}}{L_{gf}}S_{gq}$$

$$\dot{\tilde{z}}_4 = \frac{\partial h_4(x)}{\partial x}\dot{x} = \frac{1}{C}i_{dc} - \frac{1}{C}I_{gq}S_{gq} - \frac{1}{C}I_{gd}S_{gd} \tag{17}$$

If the system (17) has linear control inputs of $\tilde{v}_1$, $\tilde{v}_2$, $\tilde{v}_3$ and $\tilde{v}_4$, we can write the following:

$$\tilde{v}_1 = \omega_o I_{rd} + \frac{R_{rf}}{L_{rf}}I_{rq} + \frac{V_{rq}}{L_{rf}} - \frac{v_{dc}}{L_{rf}}S_{rq}$$

$$\tilde{v}_2 = \frac{R_{rf}}{L_{rf}}I_{rd} - \omega_o I_{rq} + \frac{V_{rd}}{L_{rf}} - \frac{v_{dc}}{L_{rf}}S_{rd}$$

$$\tilde{v}_3 = -\omega_o I_{gd} - \frac{R_{gf}}{L_{gf}}I_{gq} - \frac{V_{gq}}{L_{gf}} + \frac{v_{dc}}{L_{gf}}S_{gq}$$

$$\tilde{v}_4 = \frac{1}{C}i_{dc} - \frac{1}{C}I_{gq}S_{gq} - \frac{1}{C}I_{gd}S_{gd} \tag{18}$$

A standard linear control theory can be applied to obtain the inputs for the linear controller as follows:

$$\tilde{v}_1 = k_{1p}\left(I_{rq_{ref}} - I_{rq}\right) + k_{1i}\int_0^t \left(I_{rq_{ref}} - I_{rq}\right)dt$$

$$\tilde{v}_2 = k_{2p}\left(I_{rd_{ref}} - I_{rd}\right) + k_{2i}\int_0^t \left(I_{rd_{ref}} - I_{rd}\right)dt$$

$$\tilde{v}_3 = k_{3p}\left(I_{gq_{ref}} - I_{gq}\right) + k_{3i}\int_0^t \left(I_{gq_{ref}} - I_{gq}\right)dt$$

$$\tilde{v}_4 = k_{4p}\left(v_{dc\_ref} - v_{dc}\right) + k_{4i}\int_0^t \left(v_{dc\_ref} - v_{dc}\right)dt \tag{19}$$

where the subscript *'ref'* denotes the reference value of the corresponding variable.

Gains are tuned in the following way to make the outputs follow their respective reference values so that the error is minimized:

$$k_{1p} = 2I_{rq\_ref}k_{2p} = 2I_{rd\_ref}$$

$$k_{3p} = 2I_{gq\_ref}k_{4p} = 2v_{dc\_ref}$$

$$k_{1i} = I^2_{rq\_ref}k_{2i} = I^2_{rd\_ref}$$

$$k_{3i} = I^2_{gq\_ref}k_{4i} = v^2_{dc\_ref}$$

The values of I_{rq_ref}, I_{rd_ref}, I_{gq_ref} and v_{dc_ref} are calculated from P_{r_ref} and Q_{r_ref} given by MPPT of the DFIG at 'normal' mode as follows [39]:

$$I_{rq_{ref}} = \frac{2}{3}\frac{P_{r_{ref}}}{V_{rq}}$$

$$I_{rd_{ref}} = \frac{2}{3}\frac{Q_{r_{ref}}}{V_{rd}}$$

$$I_{gq_{ref}} = \frac{2}{3}\frac{P_{r_{ref}}}{V_{gq}}$$

$$v_{dc\_ref} = \frac{P_{r\_ref}}{i_{dc}} \tag{20}$$

When V becomes less than the V_{TH_LVRT}, then the 'LVRT mode' activates with MPPT calculating the values of I_{rq_ref}, I_{rd_ref}, I_{gq_ref} and v_{dc_ref} as:

$$I_{rq_{ref}} = \frac{2}{3}\frac{P_{r_{ref}}}{V_{rq}} + K_{RSC_{FRT}}\left(V_{TH_{FRT}} - V\right)$$

$$I_{rd_{ref}} = \frac{2}{3}\frac{Q_{r_{ref}}}{V_{rd}}$$

$$I_{gq_{ref}} = \frac{2}{3}\frac{P_{r_{ref}}}{V_{gq}}$$

$$v_{dc\_ref} = \frac{P_{r\_ref}}{i_{dc}} + K_{GSC\_FRT}\left(V_{TH\_FRT} - V\right) \tag{21}$$

From (18), the control law for the RSC can be obtained as follows:

$$S_{rq} = \frac{L_{rf}}{v_{dc}}\left(\tilde{v}_1 + \omega_o I_{rd} + \frac{R_{rf}}{L_{rf}}I_{rq} + \frac{V_{rq}}{L_{rf}}\right)$$

$$S_{rd} = \frac{L_{rf}}{v_{dc}}\left(\tilde{v}_2 + \frac{R_{rf}}{L_{rf}}I_{rd} - \omega_o I_{rq} + \frac{V_{rd}}{L_{rf}}\right) \tag{22}$$

Meanwhile, the control law for the GSC:

$$S_{gq} = \frac{L_{gf}}{v_{dc}}\left(\tilde{v}_3 + \omega_o I_{gd} + \frac{R_{gf}}{L_{gf}}I_{gq} + \frac{V_{gq}}{L_{gf}}\right)$$

$$S_{gd} = -\frac{C}{I_{gd}}\left(\tilde{v}_4 - \frac{i_{dc}}{C} + \frac{L_{gf}I_{gq}}{Cv_{dc}}\left(\tilde{v}_3 + \omega_o I_{gd} + \frac{R_{gf}}{L_{gf}}I_{gq} + \frac{V_{gq}}{L_{gf}}\right)\right) \tag{23}$$

A flowchart of the proposed control design procedure has been provided in Fig. 2.

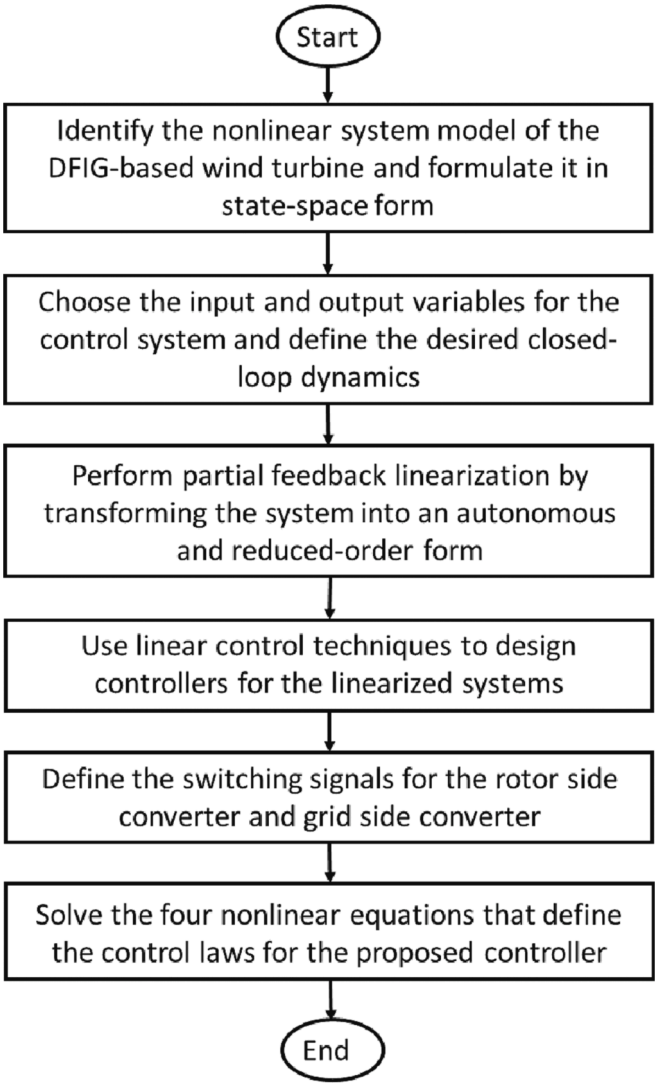

Fig. 2. Flow chart of the proposed control design procedure.

4. Controller implementation

In this section, the software implementation procedure of the proposed control scheme has been discussed in PSCAD/EMTDC platform. Fig. 3 shows the implementation block diagram of the proposed control scheme.

A phase-locked loop (PLL) has been adopted from the work presented in [44] and utilized for grid synchronization to an angular frequency ω_o. A standard model of an additional protection scheme from PSCAD/EMTDC library has been implemented to monitor the inrush rotor current and make tripping decisions based on its threshold. All voltage and current flows across the loop of the power electronic converters (RSC and GSC) have been converted into corresponding q and d-axis components. MPPT equations (Eq. (20) for 'normal mode' and Eq. (21) for 'LVRT mode') and linear controller equations (19), on the other hand, have been used to obtain the linear control input signals $\tilde{v}_1$, $\tilde{v}_2$,$\tilde{v}_3$ and $\tilde{v}_4$. All these signals have been used by the control laws (22)-(23) for generating switching signals in qd frame. Finally, these switching signals have been fed to both the converters through pulse width modulation (PWM).

A sinusoidal PWM (SPWM) technique has been used in this work, where the modulation index is a function of V_g and v_{dc}. To prevent overmodulation, v_{dc} has been selected in a way so that the following inequality constraint always holds:

$$V_g \leq v_{dc}/2 \tag{24}$$

This action might not be sufficient under the worst-case scenario when P_{ref} and Q_{ref} have a high rate of change. In such cases, a rate limiter has been used with the proposed damping controller to prevent overmodulation.

5. Controller performance assessment

In this section, the performance of the proposed PFL controller in augmenting LVRT capability of DFIG wind turbines has been assessed through electromagnetic transient simulations in PSCAD/EMTDC platform. Table 2 gives simulation data for the power system used in this paper.

Table 2
Power system simulation data.

Parameter	Symbol	Value	Unit
Nominal power	P	148	MW
Nominal voltage (line to line)	$V_{L\text{-}L}$	690	V
Nominal frequency	f	50	Hz
Stator leakage resistance	R_s	0.0084	p.u.
Stator leakage inductance	L_s	0.167	p.u.
Rotor leakage resistance	R_r	0.0083	p.u.
Rotor leakage inductance	L_r	0.1323	p.u.
Turbine inertia constant	H_t	2.5	p.u.
Generator inertia constant	H_g	0.5	p.u.
Turbine damping coefficient	D_t	2.5	p.u.
Generator damping coefficient	D_g	0.5	p.u.
Stiffness coefficient	K_s	0.15	p.u.
Slip	s	0.02	–
Converter maximum power	P_{cmax}	0.5	p.u.
GSC filter resistance	R_{gf}	0.0015	p.u.
GSC filter inductance	L_{gf}	0.15	p.u.
Nominal DC-link voltage	v_{dc}	1450	V
DC-link capacitance	C	10,000	μF
Transformer inductance	L_{tr}	0.0005	p.u.
Transmission line resistance	R	0.02	p.u.
Transmission line inductance	L	0.0016	p.u.
Compensator capacitance	C_{sc}	10,000	μF
Grid capacity	S_{Grid}	1000	MVA

5.1. LVRT performance assessment

The performance of the proposed PFL controller has been compared to that of a commercial PI controller in augmenting LVRT capability of DFIG wind turbines. The comparison has been carried out in terms of several parameters, including active power, reactive power and voltage at PCC, DC-link voltage, stator voltage, stator current, rotor voltage, rotor current, rotor angular speed, and mechanical torque during both symmetric and asymmetric LVRT conditions. The comparison has aimed to assess the control performance in terms of key metrics such as recovery time, rise time, settling time, overshoot, peak magnitude, steady-

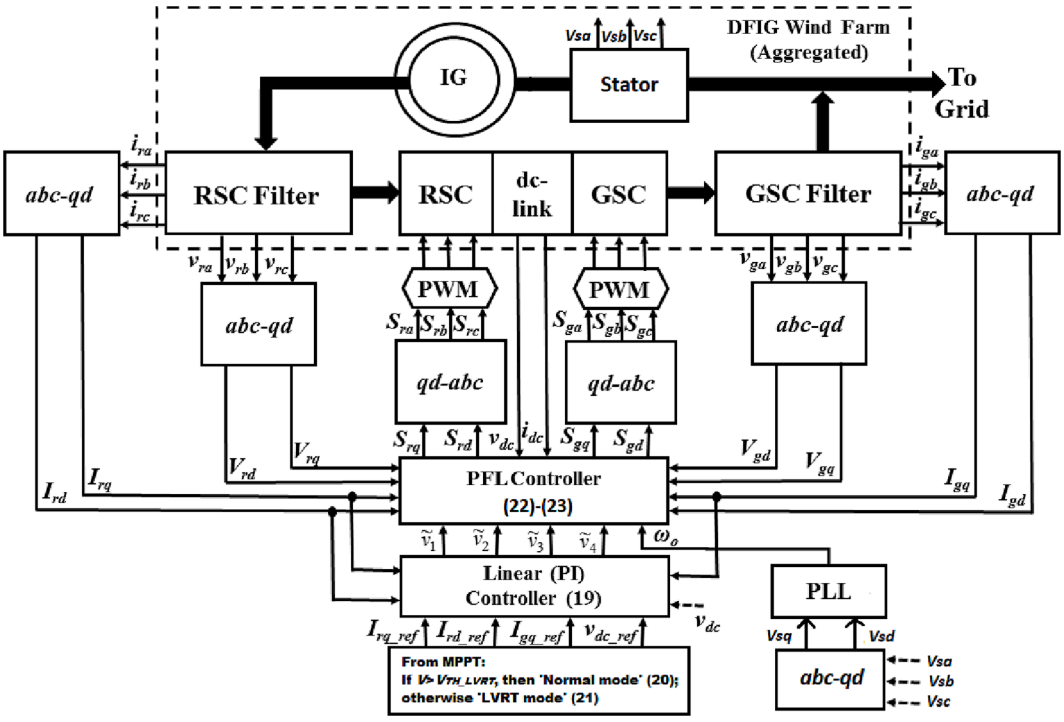

Fig. 3. Implementation block diagram of the proposed control scheme.

state error, and damping ratio.

A constant wind speed has been considered in the simulation study since system oscillation due to a fault or any other abnormal condition fluctuates much faster as compared to wind speed variations. Table 3 gives the simulation settings.

5.1.1. Symmetric LVRT

A symmetric three-phase-to-ground fault has been simulated at 1 s, which has been cleared by primary protection fault clearance time (120 ms) as shown in Fig. 4. The PPC voltage has experienced a dip of about 90 % within the fault duration that has activated the 'LVRT mode' in the proposed controller (as soon as the PPC voltage has passed below $V_{TH\_LVRT} = 0.8$ pu). Both controllers have demonstrated a similar voltage rise time of 0.28 s. However, the proposed controller has been observed to respond quickly to restore the voltage to its pre-fault value with a settling time of 0.81 s after the fault clearance. In comparison, the PI controller has exhibited a longer settling time of 1.13 s.

Due to the voltage dip during the fault, the active power output has tended to drop to zero. The proposed controller has maintained the active power output within a narrow range, which is essential for ensuring stable grid operation. After the fault clearance, the active power has started to recover. The proposed controller has displayed a faster recovery time of 0.76 s while the PI controller took 1.12 s. Additionally, the proposed controller has performed better with an overshoot of 17.11 % and a settling time of 2.16 s as opposed to an overshoot of 19.74 % and a settling time of 2.6 s for the PI controller.

With the PCC voltage dip, the reactive support has been ensured through the advanced algorithm programmed for 'LVRT mode' in the proposed controller for quick system restoration. The proposed controller has potentially eliminated the reactive power overshoot through efficient energy discharging. The proposed controller also has demonstrated a settling time of 1.9 s compared to 2.3 s for the PI controller.

The proposed controller has demonstrated effective regulation of the DC-link voltage during voltage dips. This helps to ensure stable power transfer between the RSC and GSC, which is crucial for maintaining proper grid operation. When using the proposed controller, the DC-link voltage has not exceeded 10 % of the nominal value. In contrast, when using the PI controller, the DC-link voltage has been observed to exceed 21 % of the nominal value. Additionally, the PI controller has been found to be slow in responding to fluctuations in the DC-link voltage, which may potentially pose a risk of converter failure.

The proposed controller has demonstrated to regulate the stator and rotor voltages to maintain stable operation during voltage dips. On the other hand, the PI controller has been observed to have a slow response time in recovering the pre-fault values of stator and rotor voltages. Results have shown that the proposed controller has achieved settling time of 0.78 s for stator voltage and 1.6 s for rotor voltage. In contrast, the PI controller has exhibited longer settling time of 1.09 s for stator voltage and of 1.98 s for rotor voltage.

With the PI controller, the stator and rotor currents have reached the peak magnitude at about 2p.u. and 1.15p.u., respectively. The proposed controller, on the other hand, has been found to effectively limit the stator and rotor currents during voltage dips, thereby minimizing potential risk of converter failure.

The reduction in active power due to voltage dip during the fault has been compensated through acceleration of rotor angular speed. The proposed controller has been observed to effectively restrict the speed of the wind turbine within 5.35 % of the nominal value, whereas the PI controller has been found to exceed the limit by about 6.5 %. The proposed controller also has demonstrated a steady-state error of 0.6 % as compared to that of 0.92 % for the PI controller.

After the fault clearance, the sudden restoration of the power system has resulted in a sudden change in the electrical power output. This has caused a momentary change in the turbine's mechanical torque leading to torsional oscillations. Both controllers have demonstrated a similar damping ratio of 0.86. However, the proposed controller has acted quicker in damping the oscillation and thereby reducing the mechanical stress on the turbine blades as compared to the PI controller.

Table 3
Simulation settings.

Parameter	V_W	V_{TH_LVRT}	K_{RSC_LVRT}	K_{GSC_LVRT}
Values	13 m/s	0.8 p.u.	1	12.4

5.1.2. Asymmetric LVRT

A simulation of an asymmetric line-to-line-to-ground fault has been conducted and cleared by circuit breaker fail protection fault clearance time (430 ms), as shown in Fig. 5. The PPC voltage has encountered a dip of about 65 % within the fault duration that has activated the 'LVRT mode' in the proposed controller. Both controllers have demonstrated a similar voltage rise time of 0.25 s. However, the proposed controller has responded quickly to restore the voltage to its pre-fault value with a settling time of 0.51 s after the fault clearance as compared to the PI controller's longer settling time of 1.04 s.

The proposed controller has exhibited a faster active power recovery time of 0.37 s as compared to 0.41 s with the PI controller after the fault clearance. Despite exhibiting similar overshoot of 18.6 %, the proposed controller has outperformed the PI controller with a settling time of 1.67 s as compared to the latter's settling time of 2.08 s.

Through efficient energy discharging, the proposed controller has shown promising results in potentially eliminating the reactive power overshoot. Furthermore, the proposed controller has demonstrated a quicker settling time of 1.68 s in comparison to 2.08 s with the PI controller.

The proposed controller has demonstrated effective regulation of the DC-link voltage during voltage dips, preventing it from exceeding 7 % of the nominal value. In contrast, the PI controller has allowed the DC-link voltage to exceed 21 % of the base value and has been slow in responding to fluctuations in the voltage risking potential converter failure.

The proposed controller has also regulated the stator and rotor voltages to maintain stable operation during voltage dips. Despite exhibiting similar settling times for rotor voltages of 1.19 s, the proposed controller has achieved a faster settling time for stator voltage of 0.57 s as compared to 0.97 s with the PI controller.

The stator and rotor currents have appeared to hit the peak at about 2.1 p.u. and 1.1p.u., respectively, with the PI controller. The proposed controller, on the other hand, has been found to restrict these quantities to smaller values minimizing the potential risk of converter failure.

The acceleration of rotor angular speed the reduction in active power has been effectively compensated by the proposed controller. It has restricted the wind turbine speed within 6.7 % of the nominal value while the PI controller has exceeded the limit by up to 8.6 %. The proposed controller has also demonstrated a lower steady-state error of 0.57 % than that of 0.78 % with the PI controller.

The proposed controller has effectively dampened the momentary torsional oscillation experienced by the mechanical torque, exhibiting a higher damping ratio of 0.9 in comparison to the PI controller's damping ratio of 0.83. The proposed controller also has stabilised the system quicker as compared to the PI controller.

5.2. Robustness assessment

The robustness of the proposed PFL controller for DFIG wind turbines has been assessed by examining its capacity to handle parametric variations like wind speed variations, and withstand disturbances caused by different voltage dips. A symmetric fault with a duration of 120 ms has been considered for the assessment. The comparison has been carried out in terms of active power, reactive power, and voltage at the PCC.

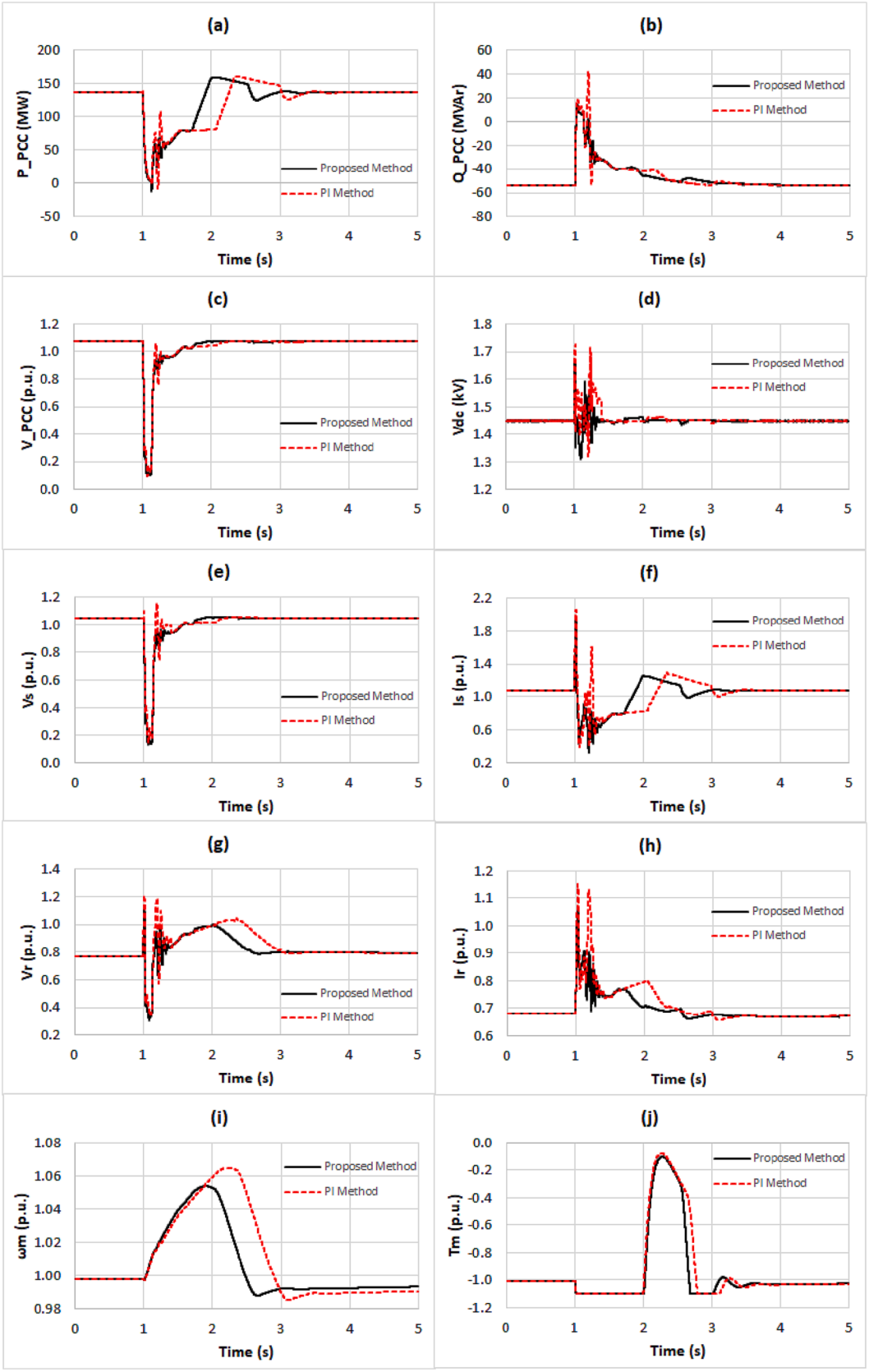

Fig. 4. DFIG's symmetric LVRT response with the proposed PFL and the PI controller: (a) PCC Active Power, (b) PCC Reactive Power, (c) PCC voltage, (d) DC-link Voltage, (e) Stator Voltage, (f) Stator Current, (g) Rotor Voltage, (h) Rotor Current, (i) Rotor Angular Speed and (e) Mechanical Torque.

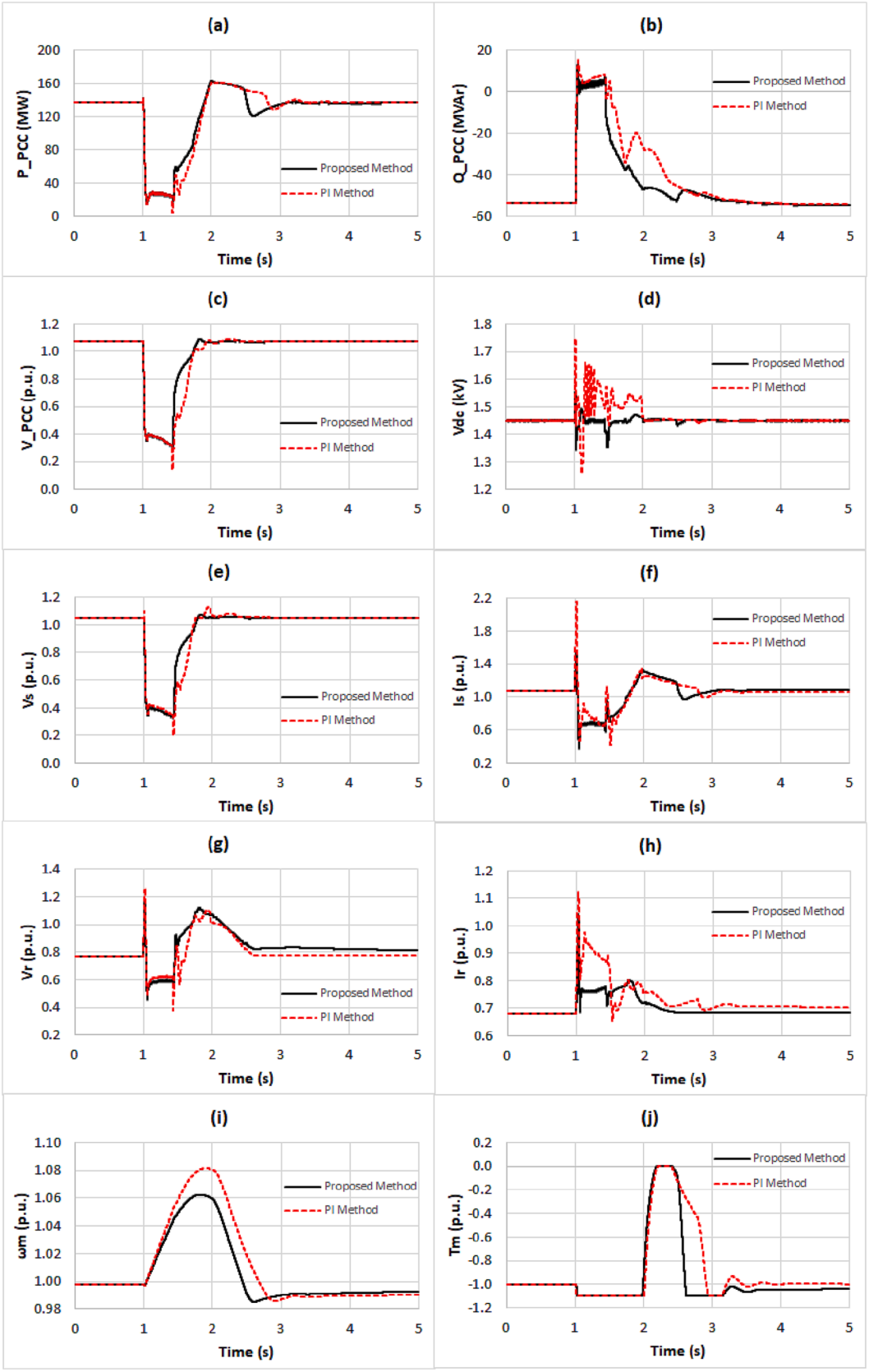

Fig. 5. DFIG's asymmetric LVRT response with the proposed PFL and the PI controller: (a) PCC Active Power, (b) PCC Reactive Power, (c) PCC voltage, (d) DC-link Voltage, (e) Stator Voltage, (f) Stator Current, (g) Rotor Voltage, (h) Rotor Current, (i) Rotor Angular Speed and (e) Mechanical Torque.

5.2.1. Wind speed variations

The transient performance of the proposed controller has been assessed under wind speeds of 12 m/s, 13 m/s, and 14 m/s, respectively, as shown in Fig. 6. The proposed controller has been found to maintain stable operation across the different wind speeds. Specifically, the controller has been able to regulate the active power and reactive power of the DFIG within acceptable limits while maintaining the voltage at the PCC close to the nominal value. With the proposed controller, the DFIG has generated required reactive power for voltage recovery even at higher wind speeds. This has occurred without affecting the overall performance of the controller demonstrating its ability to adapt itself to varying operating conditions. Based on these findings, the proposed controller has proven to be robust for DFIG wind turbines. This is indicative of the controller's capability of handling different wind speeds and maintaining stable operation in the presence of varying wind conditions.

5.2.2. Voltage dip variations

The transient performance of the proposed controller has been assessed for varying voltage dips of 90 %, 50 %, and 20 %, respectively, as shown in Fig. 7. The simulation results have demonstrated that the proposed controller has been able to accurately regulate the DFIG's active and reactive power outputs as well as the voltage level at the PCC under all tested voltage dips. The controller has also exhibited a quick response to voltage dips maintaining stable operation. Furthermore, the proposed controller has provided reliable and robust regulation of the DFIG's reactive power output. As indicated by these findings, the proposed controller has demonstrated to be a promising control strategy for DFIG wind turbines in terms of robustness against varying voltage dips.

5.3. Comparison with the existing nonlinear control techniques

A comparative study among different nonlinear control techniques and the proposed PFL method has been conducted. To ensure comparability among the investigated nonlinear control-based techniques for LVRT enhancements, no additional hardware, components, or ESS has been employed. The comparison has been illustrated in Table 4 based on the controller's ability in regulating dynamic performances of DFIG wind turbines. As indicated by these results, the proposed controller has demonstrated superior performance as compared to the other existing nonlinear control techniques.

6. Conclusions

A nonlinear controller has been proposed in this paper using partial feedback linearization (PFL) technique to augment the low voltage ride through (LVRT) capability of Doubly Fed Induction Generator (DFIG)-based wind turbines over a wide range of operating conditions. The controller generates simultaneous switching signals for both the rotor side converter and the grid side converter to restrain rotor current, dampens out stator voltage oscillations, and maintain DC-link voltage due to voltage dips during faults.

The proposed PFL method has been implemented into a partially linearized form of a nonlinear system, where the transformed system has been made autonomous and reduced in order. All calculations in the proposed method except for the control laws have been carried out offline resulting in reduced design and implementation complexity. This has allowed real-time solution requirement of small number of nonlinear equations leading to small computational burden and offline control tuning with fast tracking performances. The proposed control has been designed and implemented in several sequential steps like system modeling and partial linearization, control law derivation, software implementation, and control tuning.

The performance of the proposed controller has been compared to that of a commercial PI controller in augmenting LVRT capability of DFIG wind turbines under both symmetric and asymmetric fault

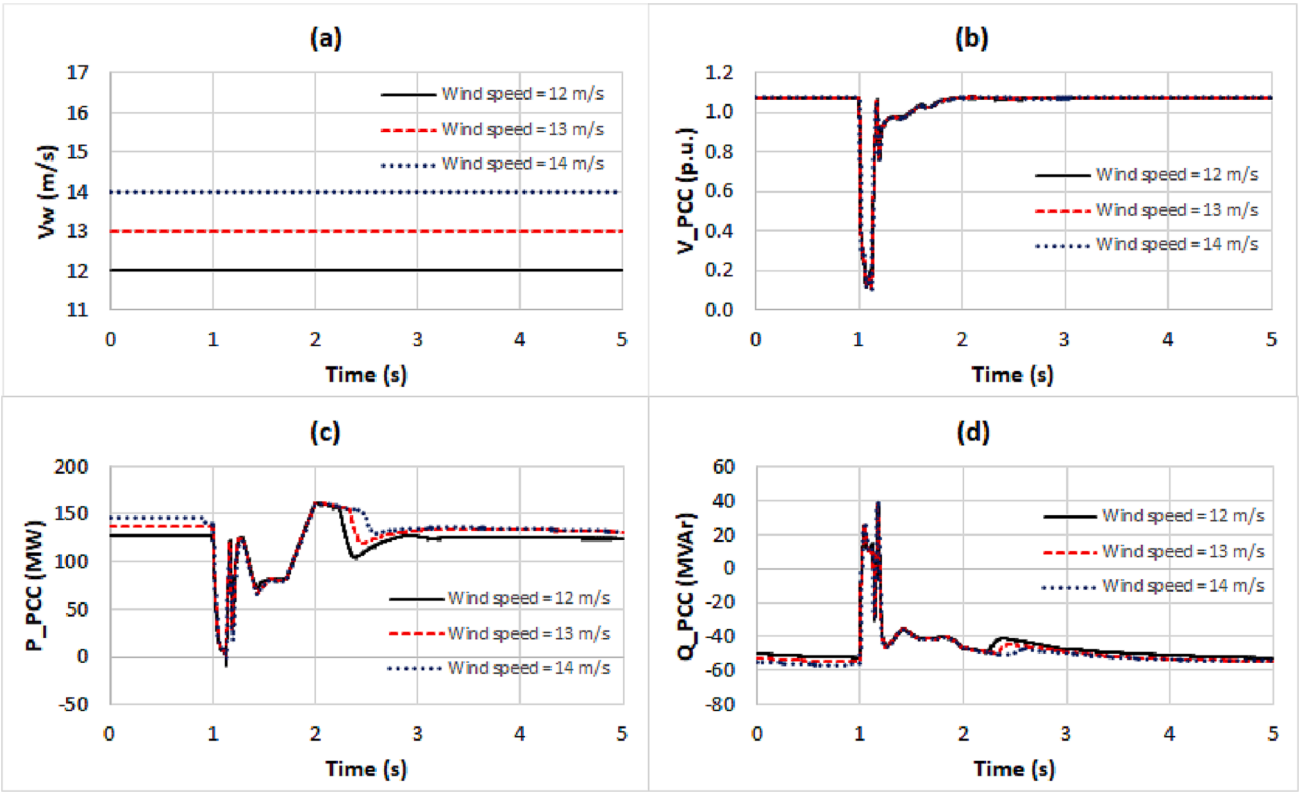

Fig. 6. DFIG's transient response under wind speed of 12 m/s, 13 m/s and 14 m/s with the proposed controller: (a) Wind Speed, (b) PCC voltage, (c) PCC Active Power and (d) PCC Reactive Power.

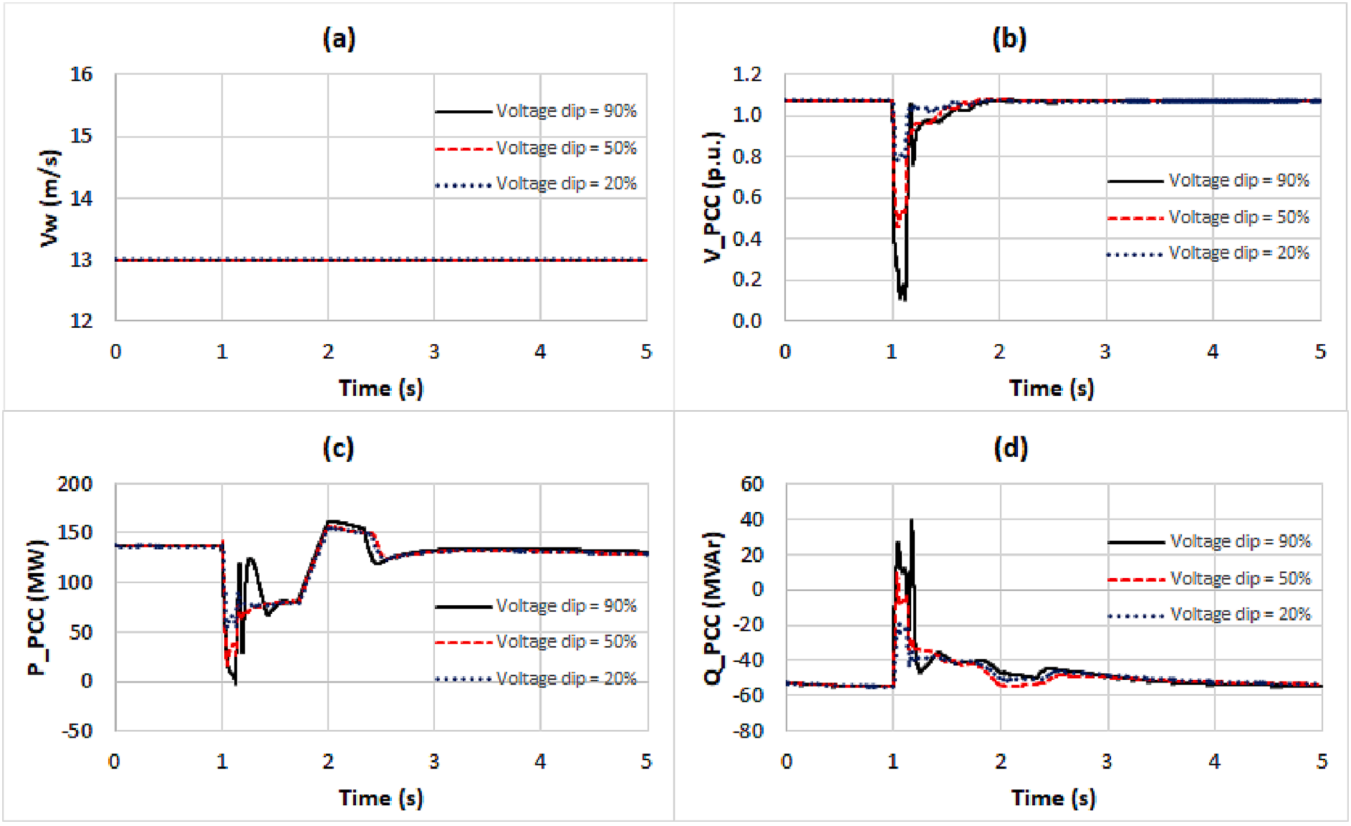

Fig. 7. DFIG's transient response for voltage dips of 90 %, 50 % and 20 % with the proposed controller: (a) Wind Speed, (b) PCC voltage, (c) PCC Active Power and (d) PCC Reactive Power.

Table 4
Comparison of different nonlinear control techniques for LVRT enhancements.

Nonlinear Control Techniques	LVRT Features							
	High Stator Current	**High Rotor Current**	**Stator Current Oscillation**	**Rotor Current Oscillation**	**High DC Link Voltage**	**High Rotor Speed**	**Torque Oscillation**	**Post Fault Recovery**
Fuzzy Adaptive Internal Model Controller [25]	Yes 200 %	Yes 200 %	Yes	Yes	NA	No 3.5 %	Yes 180 % Overshoot	Slow and Oscillatory
Model Predictive Control [26]	NA	Yes 140 %	NA	Yes	No 5–10 % Oscillatory	No 10 %	NA	Slow and Oscillatory
Model Predictive Fuzzy Control [28]	NA	Yes 220 %	NA	Yes	Yes 17.4 %	NA	NA	Faster but Oscillatory
Adaptive Back Stepping Controller [30]	NA	NA	NA	NA	No 2.61 %	NA	NA	Fast
Sliding Mode Control + Feedback Linearization [31]	NA	Yes 250 %	NA	Yes	Yes 13 %	No 10 %	Yes 2–5 % Overshoot	Slow and Oscillatory
Sliding Mode Control [32]	Yes 400 % (peak)	Yes 600 % (peak)	Yes	Yes	Yes 16 %	NA	Yes ±200 %	Faster but Oscillatory
Sliding Mode Control + Hardware [32]	Yes 300 % (peak)	Yes 350 % (peak)	Yes	Yes	No 10 %	NA	Yes ±120 %	Faster but Oscillatory
Proposed PFL Controller	**No** **90 %**	**No** **40 %**	**Yes**	**Yes**	**No** **9 %**	**No** **5 %**	**No** **Zero** **Overshoot**	**Slower but less Oscillatory**

conditions. The proposed controller has shown to be more effective in restoring the voltage to its pre-fault value with a faster rise time and shorter settling time. It has also maintained stable grid operation during voltage dips with a faster recovery time, reduced overshoot, and settling time. The proposed controller has effectively regulated the DC-link voltage and stator and rotor voltages and restricted stator and rotor currents, and the wind turbine speed within acceptable range. The proposed controller also has responded fast in dampening torsional oscillations resulted from sudden restoration of the power system, thereby effectively reducing the mechanical stress on the turbine blades. Overall,

the proposed controller has successfully augmented the LVRT capability of DFIG wind turbines.

The robustness of the proposed controller has also been assessed. It is found robust for DFIG wind turbines with the ability to handle and maintain stable operation in the presence of diverse wind conditions and voltage sags.

The scope of future works includes the following:

- hardware-in-the-loop validation in a real-world scenario
- determination of a practical and efficient way of measuring the voltage of the rotor located downstream of the filter
- robustness analysis under model uncertainty
- extension of the proposed controller to other types of wind turbines, such as direct-drive or permanent magnet synchronous generators

CRediT authorship contribution statement

M.A. Chowdhury: Conceptualization, Methodology, Visualization, Formal analysis, Investigation, Software, Writing – original draft, Writing – review & editing. **G.M. Shafiullah:** Methodology, Formal analysis, Investigation, Supervision, Writing – review & editing. **S.M. Ferdous:** Formal analysis, Writing – review & editing.

Declaration of Competing Interest

The authors declare that they have no known competing financial interests or personal relationships that could have appeared to influence the work reported in this paper.

Data availability

No data was used for the research described in the article.

References

[1] Chuangpishit S, Tabesh A, Moradi-Sharbabk Z, Saeedifard M. Topology Design for Collector Systems of Offshore Wind Farms with Pure DC Power Systems. IEEE Trans Ind Elect 2014;61(1):320–8.

[2] Jabbour N, Tsioumas E, Mademlis C, Solomin E. A Highly Effective Fault-Ride-Through Strategy for a Wind Energy Conversion System with a Doubly Fed Induction Generator. IEEE Trans Pow Elect Aug 2020;35(8):8154–64.

[3] Spinato F, Tavner PJ, Bussel GJWV, Koutoulakos E. Reliability of wind turbine subassemblies. IET Ren Pow Gen Dec 2009;3(4):387–401.

[4] Islam MR, Hasan J, Shipon MRR, Sadi MAH, Abuhussein A, Roy TK. Neuro Fuzzy Logic Controlled Parallel Resonance Type Fault Current Limiter to Improve the Fault Ride Through Capability of DFIG Based Wind Farm. IEEE Access 2020;8:115314–34.

[5] Ma Y, Zhu D, Zou X, Kang Y, Guerrero JM. Transient Characteristics and Quantitative Analysis of Electromotive Force for DFIG-based Wind Turbines during Grid Faults. Chin Jour Elect Eng Jun 2022;8(2):3–12.

[6] Chen W, Xu D, Zhu N, Chen M, Blaabjerg F. Control of Doubly-Fed Induction Generator to Ride-Through Recurring Grid Faults. IEEE Trans Pow Elect Jul 2016;31(7):4831–46.

[7] Kenan DM. A new approach for low voltage ride through capability in DFIG based wind farm. Int Jour Elect Pow Ener Syst Sep 2016;83:251–8.

[8] Naderi SB, Negnevitsky M, Jalilian A, Hagh MT, Muttaqi KM. Optimum resistive type fault current limiter: An efficient solution to achieve maximum fault ride-through capability of fixed-speed wind turbines during symmetrical and asymmetrical grid faults. IEEE Trans Ind App Jan/Feb 2017;53(1):538–48.

[9] Din Z, Zhang J, Xu Z, Zhang Y, Zhao J. Low voltage and high voltage ride-through technologies for doubly fed induction generator system: Comprehensive review and future trends. IET Ren Pow Gen Feb 2021;15(3):614–30. https://doi.org/10.1049/rpg2.12047.

[10] Hossain MJ, Saha TK, Mithulananthan N, Pota HR. Control Strategies for Augmenting LVRT Capability of DFIGs in Interconnected Power Systems. IEEE Trans Ind Elect 2013;60(6):2510–22.

[11] Yang L, Xu Z, Ostergaard J, Dong ZY, Wong KP. Advanced Control Strategy of DFIG Wind Turbines for Power System Fault Ride Through. IEEE Trans Pow Syst 2012;27(2):713–22.

[12] Liang J, Qiao W, Harley RG. Feed-Forward Transient Current Control for Low-Voltage Ride-Through Enhancement of DFIG Wind Turbines. IEEE Trans Ener Conv 2010;25(3):836–43.

[13] Chen S, Yao J, Pei J, Liu Y, Liu R, Huang S, et al. Transient Stability Analysis and Improved Control Strategy for DC-link Voltage of DFIG-Based WT during LVRT. IEEE Trans Ener Conv Jun 2022;37(2):880–91. https://doi.org/10.1109/TEC.2021.3126855.

[14] Jalilian A, Naderi SB, Negnevitsky M, Hagh MT, Muttaqi KM. Controllable DC-link fault current limiter augmentation with DC chopper to improve fault ride-through of DFIG. IET Ren Pow Gen 2017;11(2):313–24.

[15] Naderi SB, Negnevitsky M, Muttaqi KM. A Modified DC Chopper for Limiting the Fault Current and Controlling the DC-link Voltage to Enhance Fault Ride-Through Capability of Doubly-Fed Induction-Generator-Based Wind Turbine. IEEE Trans Ind App 2019;55(2):2021–32.

[16] Amalorpavaraj RAJ, Kaliannan P, Padmanaban S, Subramaniam U, V. K. Ramachandaramurthy VK. Improved Fault Ride Through Capability in DFIG Based Wind Turbines Using Dynamic Voltage Restorer With Combined Feed-Forward and Feed-Back Control. IEEE Access 2017;5:20494-503.

[17] Qiao W, Venayagamoorthy GK, Harley RG. Real-Time Implementation of a STATCOM on a Wind Farm Equipped With Doubly Fed Induction Generators. IEEE Trans Ind App 2009;45(1):98–107.

[18] Döşoğlu MK. Crowbar hardware design enhancement for fault ride through capability in doubly fed induction generator-based wind turbines. ISA Trans 2020;104, 321-28. https://doi.org/10.1016/j.isatra.2020.05.024.

[19] Haidar AMA, Muttaqi KM. Hagh MT A coordinated control approach for DC link and rotor crowbars to improve fault ride-through of DFIG-based wind turbine. IEEE Trans Ind App 2017;53(4):4073–86.

[20] Vidal J, Abad G, Arza J, Aurtenechea S. Single-Phase DC Crowbar Topologies for Low Voltage Ride Through Fulfillment of High-Power Doubly Fed Induction Generator-Based Wind Turbines. IEEE Trans Ener Conv 2013;28(3):768–81.

[21] Campos-Gaona D, Moreno-Goytia EL, Anaya-Lara O. Fault Ride-Through Improvement of DFIG-WT by Integrating a Two-Degrees-of-Freedom Internal Model Control. IEEE Trans Ind Elect 2013;60(3):1133–45.

[22] Chen L, Zhang B, Fan X. Asymmetrical Fault Ride-Through Control Strategy for Rotor-Side Converter of DFIG. IEEE Trans Ener Conv 2020;35(2):1046–53.

[23] Mohseni M, Islam SM, Masoum MAS. Impacts of Symmetrical and Asymmetrical Voltage Sags on DFIG-Based Wind Turbines Considering Phase-Angle Jump, Voltage Recovery, and Sag Parameters. IEEE Trans Pow Elect 2011;26(5):1587–98.

[24] Rahimi M, Parniani M. Transient Performance Improvement of Wind Turbines With Doubly Fed Induction Generators Using Nonlinear Control Strategy. IEEE Trans Ener Conv Jun 2010;25(2):514–25. https://doi.org/10.1109/TEC.2009.2032169.

[25] Amuthan N, Subburaj P, Melba MP. Direct model reference adaptive internal model controller for better voltage sag ride through in doubly fed induction generator wind farms. Int Jour Elect Pow Ener Syst 2013;47:255–63. https://doi.org/10.1016/j.ijepes.2012.10.064.

[26] Abdelrahem M, Mobarak MH, Kennel R. "Model predictive control for low-voltage ride through capability enhancement of DFIGs in variable-speed wind turbine systems." In: *2016 9th International Conference on Electrical and Computer Engineering (ICECE)*, 2016, pp. 70-73. doi: 10.1109/ICECE.2016.7853858.

[27] Wei J, Li C, Wu Q, Zhou B, Xu D, Huang S. MPC-based DC-link voltage control for enhanced high-voltage ride-through of offshore DFIG wind turbine. Int Jour Elect Pow Ener Syst 2021;126, Part A:106591. https://doi.org/10.1016/j.ijepes.2020.106591.

[28] Taher SA, Arani ZD, Rahimi M, Shahidehpour M. Model predictive fuzzy control for enhancing FRT capability of DFIG-based WT in real-time simulation environment. Ener Syst 2018;9:899–919. https://doi.org/10.1007/s12667-017-0252-x.

[29] Shahriari SAA, Mohammadi M, Raoofat M. A new method based on state-estimation technique to enhance low-voltage ride-through capability of doubly-fed induction generator wind turbines. Int Jour Elect Pow Ener Syst 2018;95:118–27. https://doi.org/10.1016/j.ijepes.2017.08.016.

[30] Roy TK, Mahmud MA, Islam SN, Oo AMT, Muttaqi KM. "Enhancement of Fault Ride Through Capabilities for Grid-Connected DFIG-Based Wind Farms using Nonlinear Adaptive Backstepping Controllers." In: *2018 IEEE International Conference on Power Electronics, Drives and Energy Systems (PEDES)*, 2018, pp. 1-6, doi: 10.1109/PEDES.2018.8707642.

[31] Taher SA, Dehghani Arani Z, Rahimi M, Shahidehpour M. A new approach using combination of sliding mode control and feedback linearization for enhancing fault ride through capability of DFIG-based WT. Int Trans Elect Ener Syst 2018;28:e2613.

[32] Saad NH, Sattar AA, Mansour AEAM. Low voltage ride through of doubly-fed induction generator connected to the grid using sliding mode control strategy. Ren Ener 2015;80:583–94. https://doi.org/10.1016/j.renene.2015.02.054.

[33] Döşoğlu MK. Decoupled power-based sliding mode control modeling enhancement for dynamic stability in doubly-fed induction generator-based wind turbines. Comp Elect Eng 2022;104:108448. https://doi.org/10.1016/j.compeleceng.2022.108448.

[34] Morshed MJ, Fekih A. A new fault ride-through control for DFIG-based wind energy systems. Elect Pow Syst Res 2017;146:258–69. https://doi.org/10.1016/j.epsr.2017.02.010.

[35] Morshed MJ, A. Fekih A. A Novel Fault Ride Through Scheme for Hybrid Wind/PV Power Generation Systems. IEEE Trans Sust Ener Oct. 2020;11(4):2427-36, Oct. 2020, doi: 10.1109/TSTE.2019.2958918.

[36] Din Z, Zhang J, Xu Z, Zhang Y, Zhao J. Realization of fault ride through for doubly fed induction generator system with cascade converter. Int Trans Elect Ener Syst 2021;31(3):e12792.

[37] Tilli A, Conficoni C, Hashemi A. An effective control solution for doubly-fed induction generator under harsh balanced and unbalanced voltage sags. Cont Eng Prac 2019;84:172–82. https://doi.org/10.1016/j.conengprac.2018.11.014.

[38] Xiao S, Yang G, Zhou H, Geng H. An LVRT Control Strategy Based on Flux Linkage Tracking for DFIG-Based WECS. IEEE Trans Ind Elect Jul 2013;60(7):2820–32. https://doi.org/10.1109/TIE.2012.2205354.
[39] Mahmud MA, Pota HR, Hossain MJ. Dynamic Stability of Three-Phase Grid-Connected Photovoltaic System Using Zero Dynamic Design Approach. IEEE Jour Phot 2012;2(4):564–71.
[40] Chowdhury MA, Shafiullah GM. SSR Mitigation of Series-Compensated DFIG Wind Farms by a Nonlinear Damping Controller Using Partial Feedback Linearization. IEEE Trans Pow Syst 2018;33(3):2528–38.
[41] Reigstad TI, Uhlen K. Variable Speed Hydropower for Provision of Fast Frequency Reserves in the Nordic Grid. IEEE Trans Power Syst 2021;36(6):5476–85.
[42] Li X, Huang H, Li Z, Wu Q. Doubly-fed induction generator wind farm aggregation for power system transient stability analysis. IEEE Trans Ener Conv 2016;31(3):1121–32.
[43] Mahmud MA, Hossain MJ, Pota HR, Roy NK. Robust Nonlinear Controller Design for Three-Phase Grid-Connected Photovoltaic Systems Under Structured Uncertainties. IEEE Trans Pow Del 2014;29(3):1221–30.
[44] Kaura V, Blasko V. Operation of a phase locked loop system under distorted utility conditions. IEEE Trans Ind App 1997;33(1):58–63.